Evidence of alloy formation in CoNi nanoparticles synthesized by nanosecond-pulsed discharges in liquid nitrogen

Mahmoud Trad, Alexandre Nominé, Cédric Noël, Jaafar Ghanbaja, Malek Tabbal, Thierry Belmonte

Evidence of alloy formation in CoNi nanoparticles synthesized by nanosecond-pulsed discharges in liquid nitrogen

M. Trad[1], A. Nominé[1], C. Noël[1], J. Ghanbaja[1], M. Tabbal[2], T. Belmonte[1,*]

[1]Université de Lorraine, CNRS, Institut Jean Lamour, UMR 7198, NANCY, F-54042, France

[2]Department of Physics, American University of Beirut, Riad El Solh 1107 2020, Beirut, Lebanon

* corresponding author. Email: thierry.belmonte@univ-lorraine.fr

PACS number: 52.80.Wq Discharge in liquids and solids

Keywords: Spark discharges; Submerged discharges; Time-resolved optical emission spectroscopy; Liquid nitrogen.

ABSTRACT

Producing alloy nanoparticles by discharge-assisted erosion of electrodes immersed in liquid nitrogen is possible in the cobalt-nickel system. Several electrode configurations are tested. When one nickel electrode faces one cobalt electrode, Co_xNi_{1-x} alloy nanoparticles are produced with nickel cubic nanoparticles and cobalt round-shaped faceted nanoparticles. The possibility of forming alloys is attributed to a sufficiently-long residence time of both parent clusters within the discharge and to their total miscibility. It is also possible to form sub-micrometric Co_xNi_{1-x} alloy particles when discharges between cobalt electrodes are run in liquid nitrogen loaded with nickel nanoparticles produced in a former step. Starting by discharges between Co-electrodes before Ni-electrodes does not produce any alloy. The two mechanisms responsible for alloy synthesis are discussed.

1. Introduction

Alloy nanoparticles made of cobalt and nickel are of great interest for various technology domains, including magnetism [1–3], catalysis [4, 5], optics [6, 7] and medicine [6]. Two attractive features of the Co-Ni system are the total miscibility of the two elements and close melting points (1768 K for cobalt and 1728 K for nickel). This is why the Co-Ni system can be considered as a textbook case for the investigation of alloy formation by vapour condensation of different elements. Discharges generated in liquids can produce vapours from the electrode elements that condensate in colder regions to form nanoparticles.

Only a few studies have examined the synthesis of alloy nanoparticles by discharges in non-cryogenic liquids [8–13]. None of them provide any mechanism that could define the conditions to fulfil to form these alloys. To elucidate the problem of alloy formation in pulsed discharges, our group investigated the synthesis of alloy nanoparticles in liquid nitrogen. The advantages of using this dielectric liquid are many:

- even though Rebiai *et al.* [14] discovered that liquid nitrogen can contain up to 10 ppm of water, oxidation processes in the liquid phase are negligible,
- consequently, oxidation of nanoparticles after liquid evaporation can only be due to ambient air,
- unlike oils that are converted into soot during the discharge process, liquid nitrogen does not give any by-product,
- nanoparticles can be easily removed from the liquid after evaporation
- nitrogen, whatever its state in the discharge (atomic or molecular, excited or not), does not react with metals to form nitrides, at least in the present conditions.

The following binary systems were studied: Cu–Zn [15], Cu–Ag [16], Si–Sn [17] and Ag–Cd [18]. Alloy nanoparticles could only be synthesized if electrodes were already made of an alloy – for instance $Ag_{93.8}Cu_{6.2}$ –, but their compositions were depleted in the more volatile element. No alloy formation was observed when two electrodes, each one made of a given

metal, were used – for example Ag and Cu –. In such cases, a second step based on laser irradiation of plasma-produced nanoparticles is necessary to form alloys [19].

In this work, we study the synthesis of NiCo nanoparticles by generation of discharges in liquid nitrogen using single-element electrodes made of cobalt or nickel. To the best of our knowledge, no attempt has been made to alloy these two elements by discharges in liquids.

On the other hand, from studies on non-plasma processes that were used to grow cobalt or nickel nanoparticles, it was established that Co and Ni nanocrystals can adopt only two possible shapes and only one at a time that is dependent on the synthesis conditions. These nanocrystals can be:

- either nanospheres with some facets and sharp edges (see Xu *et al.* [20] for cobalt and Davar *et al.* [21] for nickel)
- or nanocubes (see Scariot *et al.* [22] for cobalt and Shviro and Zitoun [23] for nickel)

Preparations of amorphous nickel or cobalt nanoparticles also lead to nanospheres but well-rounded, without facets or edges[24].

In the present study, several process configurations were used in an attempt to generate Ni-Co alloy nanoparticles whose formation and characteristics were investigated using High Resolution Transmission Electron Microscopy (TEM). After a short description of the experimental set-up, results obtained in the different configurations will be described and conditions to form CoNi alloy nanoparticles will be specified and discussed.

2. Experimental set-up

The experimental set-up was presented in detail elsewhere [25]. Briefly, a high DC voltage power supply (Technix SR15-R-1200–15 kV–80 mA) fed a solid-state switch (Behlke HTS-301-03-GSM) connected to one pin-electrode, the other pin-electrode being grounded. The voltage rise time was 20 ns (no ballast resistor).

Electrodes made of pure nickel and pure cobalt (1 mm in diameter – 99.9 % purity) were used in pin-to-pin configuration and immersed in liquid nitrogen. Several configurations were

tested (see **supplemental material 1**): in the one-step process Co–Co, Ni–Ni and Ni–Co, and in the two-step process Co–Co followed by Ni–Ni and Ni–Ni followed by Co–Co. In any case, discharges were pulsed at 10 Hz during 30 minutes whatever the configuration. So the total treatment time is 30 min for the one-step process and 60 min for the two-step process. Two experimental parameters were varied: the applied voltage (4, 7 and 10 kV) and the discharge pulse width (from 75 to 2500 ns). Only results at 7 kV and 200 ns will be presented. Indeed, the pulse width affects only the amount of nanoparticles, similarly to the treatment time, but not their respective proportions [18] whereas the applied voltage does not lead to any appreciable change in material results within the selected range. The inter-electrode gap distance was 100 μm in all experiments. It is worth mentioning here that changing the power electrode, *i.e.* the electrode connected to the high voltage – for instance from Ni to Co in the Ni-Co configuration – leads to the same results and conclusions. It is likely because changing the power electrode only affects the initial stage of the discharge, which lasts between 2 and 5 nanoseconds typically before transition to arc, the whole process being always longer than 75 ns.

Nanoparticles are collected by sedimentation on a silicon wafer left on the bottom of the Dewar vessel. After treatment, once nitrogen has evaporated, they are transferred to a holey carbon grid before analysis by rubbing the silicon surface. Microstructure and composition of the nanoparticles are characterized by high-resolution TEM (HRTEM). HRTEM investigation is performed using a JEOL ARM 200 F cold FEG TEM/STEM operating at 200 kV (point resolution: 0.12 nm) and equipped with a GIF quantum ER model 965. High-angle dark-field imaging in scanning TEM (HAADF/STEM) and 2D elemental mapping using energy dispersive x-ray spectroscopy (EDX) are combined to obtain information about chemical composition of nanoparticles.

3. Result and discussion

Before presenting experimental results, it is useful to recall first several important features of nano-objects synthesised by nanosecond-pulsed discharges in dielectric liquid:

- Three populations of nanoparticles are usually produced (2–5 nm, 10–20 nm and > 100 nm). This third population is low in density and due to droplet expulsion from the liquid well that forms when the electrode is struck by the discharge and not by gas phase condensation, unlike the two other populations) [26].
- The formation of a shockwave at the very beginning of the discharge ignition blasts nanoparticles out of the inter-electrode gap, leading to optical emission lines that only belong to the electrode metal [27]. If nanoparticles of a given type (*e.g.* cobalt) are present in liquid nitrogen before discharges between two electrodes made of another metal (nickel), only emission lines of this second metal (nickel) will be observed during discharges.
- Gauzes of specific metals like zinc, silver or bismuth may also form (together with nanoparticles) by a previously unknown mechanism. These gauzes are only few-atomic-layer thick and can extend over hundreds of micrometres in the two other dimensions. They can be more or less porous, depending on experimental conditions.

3.1. Single element nanoparticle synthesis

Figure 1 shows TEM bright field images of air-oxidized nickel and cobalt nanoparticles synthesized using Ni and Co electrodes, respectively.

As mentioned previously, oxidation of nanoparticles by ambient air is the only significant oxidation mechanism that occurs once liquid nitrogen has evaporated and left nanoparticles unprotected. Rebiai *et al.* [14] discovered that the solubility of water in liquid nitrogen could be as high as 10 ppm. Then, oxidation is not impossible during the discharge process since liquid nitrogen acts a non-empty reservoir of oxidative species. Nevertheless, this effect is extremely limited because of the very low content of oxidative species in the liquid phase and

the huge specific area of nanoparticles that act as a Getter trap. Experiments made in the two-step process by wrapping copper nanoparticles with a zinc gauze in liquid nitrogen showed fully metallic copper particles, unaffected by oxidation but covered by a ZnO layer [15].

Erosion of cobalt electrodes by spark discharges in the present conditions produces spherical nanoparticles exhibiting edges whereas erosion of nickel by spark discharges leads to cubic nanoparticles.

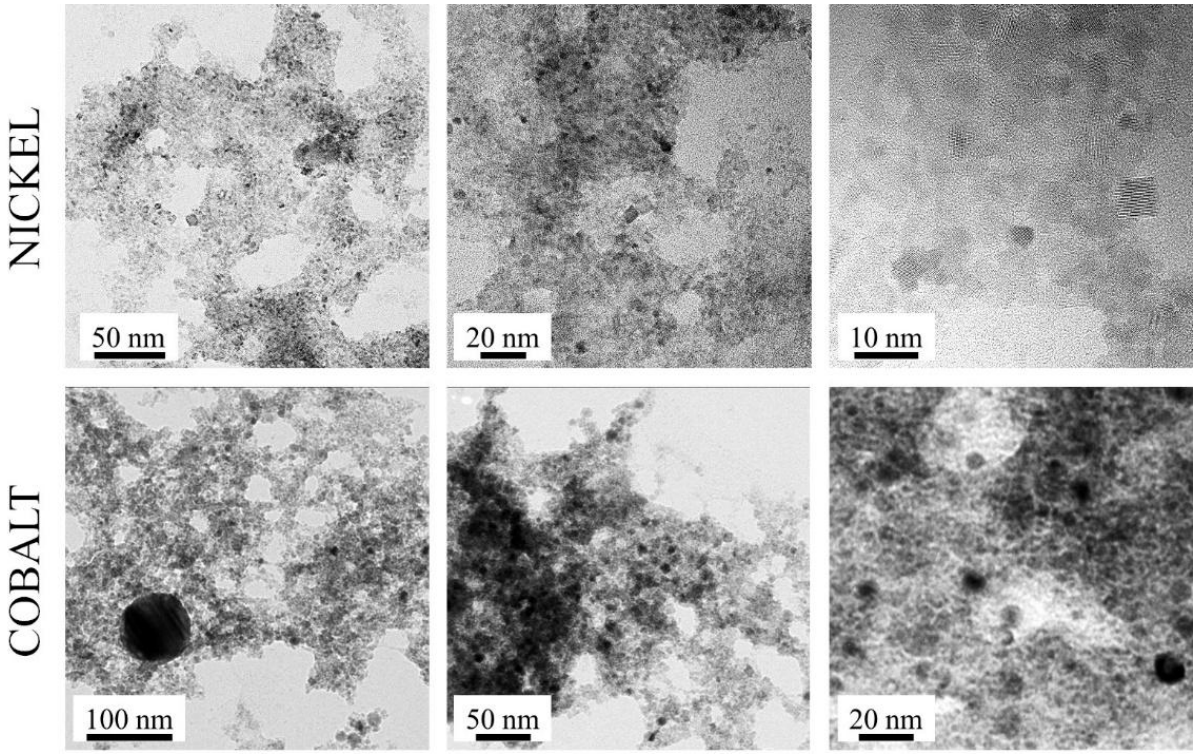

Fig. 1: Nickel and cobalt nanoparticles observed by transmission electron microscopy at different magnifications. Nickel oxide nanoparticles are cubic with sizes below 10 nm. Cobalt oxide nanoparticles appear more spherical and exhibit three size distributions, as discussed in the text.

In the case of cobalt, TEM images show the presence of crystallized nanoparticles with a size distribution between 4 and 15 nm in diameter. Another size distribution of larger nanoparticles, with diameters between 30 and 60 nm, has also been observed but with a much

lower occurrence. The third population is also present with rare particles exhibiting diameters beyond 100 nm.

Similarly, after discharges between two nickel tip electrodes, transmission electron microscopy shows crystallized nanoparticles having a size distribution between 2 and 8 nm.

Electron diffraction and Fast Fourier Transform (FFT) analyses performed with high-resolution images on individual nanoparticles confirm the chemical composition determined by energy dispersive spectroscopy. The nanoparticles are made of cobalt oxide and nickel oxide (NiO) (both being cubic centred – space group: $Fm\bar{3}m$), as expected.

From results presented in introduction, we deduce that, under the present synthesis conditions, nickel nanoparticles adopt a cubic shape whereas cobalt nanoparticles appear as spheres with some facets. Consequently, we can associate unequivocally each metal to a given shape.

3.2. Two-step sequential discharges process

Figure 2 shows TEM images of nanoparticles obtained when the process is run first during one hour with cobalt electrodes and next during another one-hour with nickel electrodes immersed in the solution that contains the formerly-grown cobalt nanoparticles [15]. No alloying between the two metals could be observed in this condition. Nickel and cobalt are mixed together, making the analysis a bit more complicated, but in some areas, they are well separated and they can be used as test particles to determine composition by EDX analyses. **Fig. 2** shows nanoparticles made of cobalt (spheres with facets) or nickel (cubes). Cobalt nanoparticles also form sheet-like agglomerated structures (referred to as gauzes hereinafter) that are slightly-porous networks of interconnected cobalt nanoparticles.

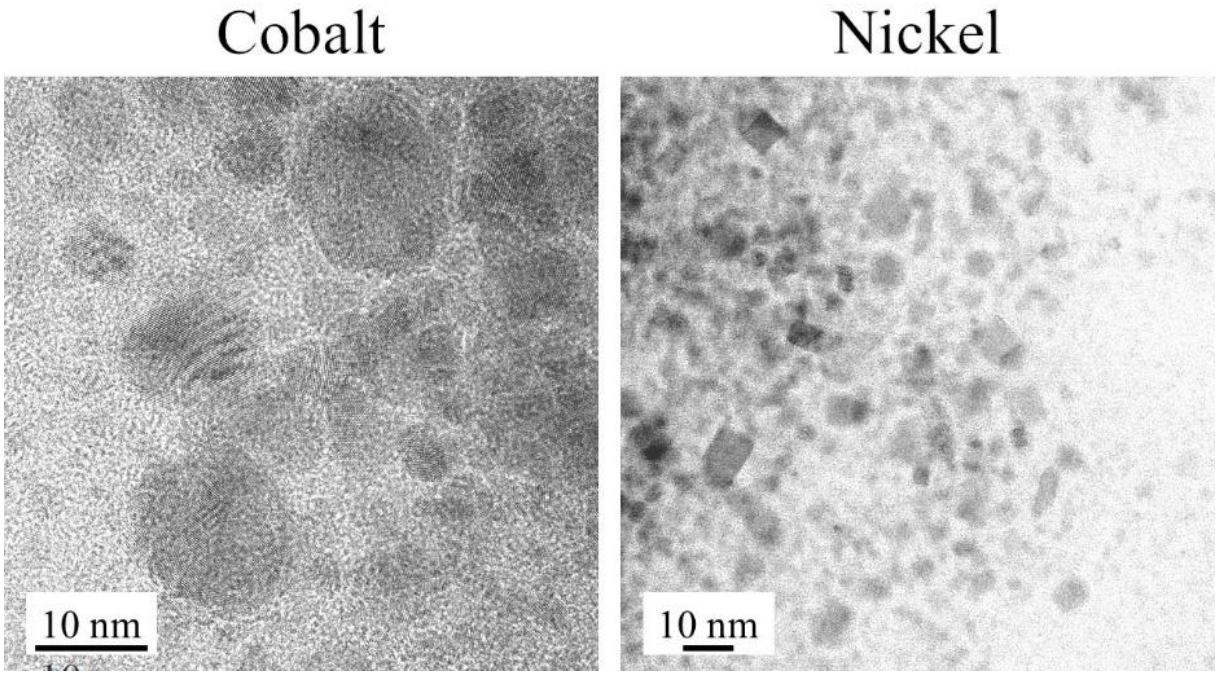

Fig. 2: TEM micrographs of cobalt and nickel nanoparticles observed after a two-step process starting with one hour of pulsed discharges in Co-Co configuration followed by one hour of pulsed discharges in Ni-Ni configuration.

As cobalt is produced during the first step of the process, nickel nanoparticles can be wrapped in cobalt gauzes, as seen in **Fig. 3**, forming a core-shell structure. This mechanism has already been observed in the Cu-Zn system, zinc forming easily gauzes [15]. The formation of these core-shell structures is very specific to the present process and requires the presence of a gauze of a given metal, *e.g.* nickel. Then, fast nanoparticles made of the other metal, here cobalt, impact the gauze at high speed, warp it and get wrapped in it. This mechanism is assumed to occur outside the discharge region because the gauze would not keep its 2D-shape in the highest temperature region where prevailing thermodynamic conditions would necessarily turn its shape to spherical.

The EDX analysis of the selected particle is reported as **Supplemental Material 2**, and suggests that the particle is essentially made of nickel (~87 at.%) with a low amount of cobalt

(< 1 at.%) and oxygen (~12 at.%). Another example, where the Co gauze can be more easily distinguished is depicted in **Supplemental Material 3.**

Actual elemental distributions are deduced from raw profiles (top graph in **Fig. 3**) by Abel's inversion (bottom graph in **Fig. 3**). This latter graph is divided into two parts:

- from –60 to 0 nm, raw data were processed after smoothing using adjacent-weighted averaging over 20 neighbouring data points.
- from 0 to +60 nm; raw data were processed without any treatment.

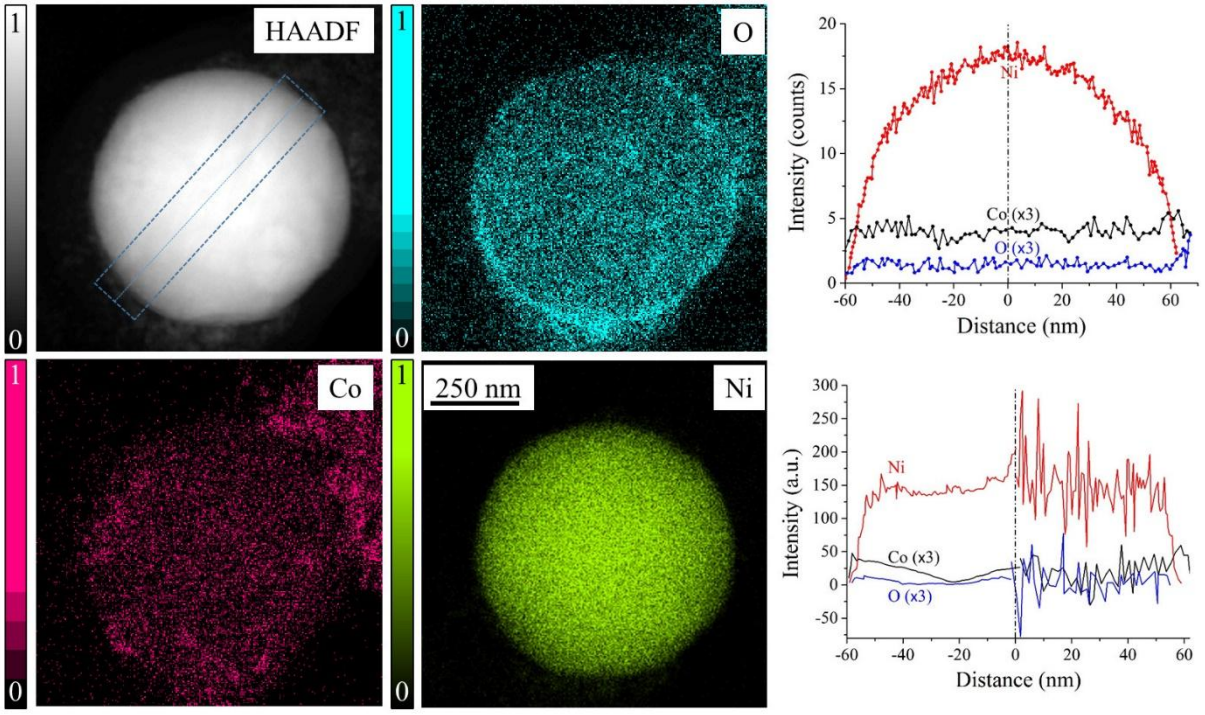

Fig. 3: STEM analysis of a nickel nanoparticle covered by cobalt oxide obtained by a two-step process starting with Co. Coloured scales are normalized element intensities. Elemental analysis (on the rhs of the figure) along a line depicted in the HAADF image shows clearly constant intensities of O and Co, contrary to nickel (top graph). The actual distribution of elements within the particle can be deduced by Abel's inversion (bottom graph – see main text for details). It is clearly a Ni-core/CoO-shell structure. The nickel nanoparticle is wrapped into a CoO gauze. It is not a segregation of cobalt in a CoNi alloy leading to a CoO layer with

a core depleted in cobalt as it will be described hereafter. The distribution of cobalt over the nickel nanoparticle is not necessarily homogeneous.

Nickel gauzes also form and must be distinguished from nickel sheets that are denser, *i.e.* formed as a whole and not as porous networks of interconnected nanoparticles, as seen in **Fig. 4**. The formation mechanism of these sheets (only found for some elements like Zn, Ag or Bi) is still unclear, though it is suspected to have to do with electrode exfoliation, a few atomic layers being detached from metal grains during the discharge process [27]. This scenario is yet to be substantiated.

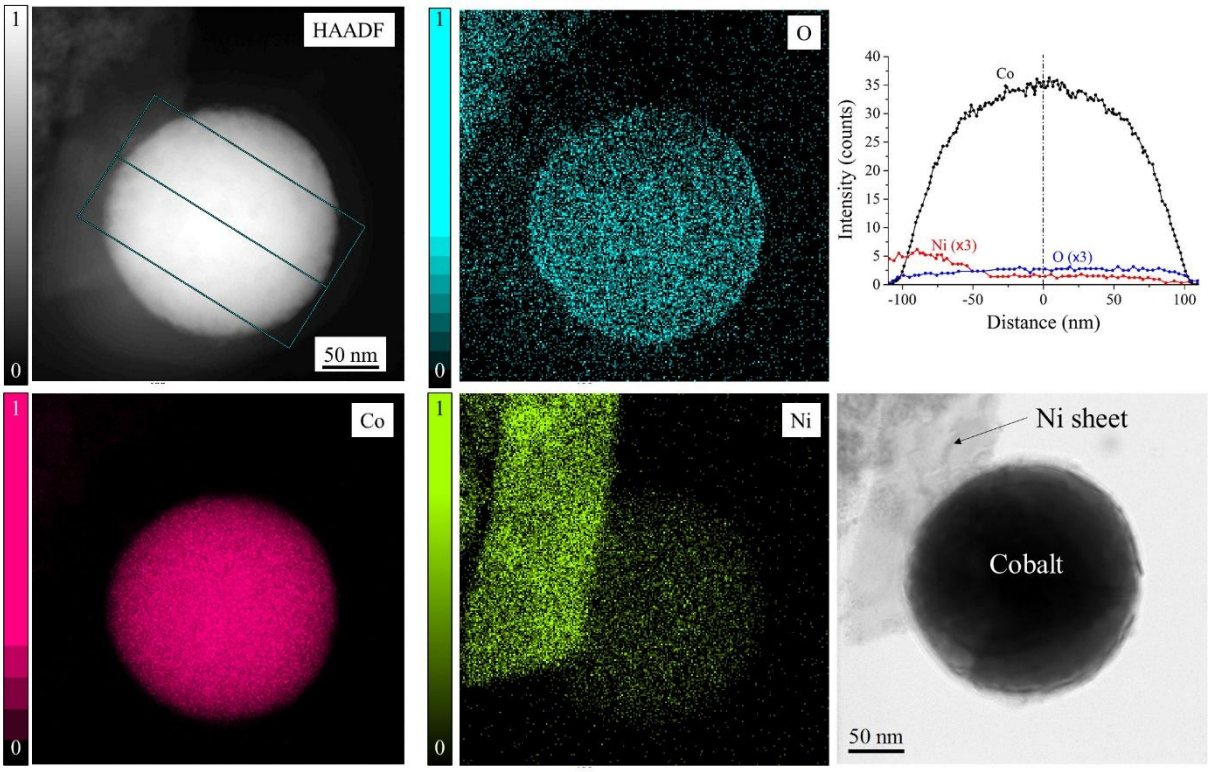

Fig. 4: STEM analysis of a cobalt nanoparticle produced by a two-step process starting with Co. Coloured scales are normalized element intensities. The nanoparticle is covered by a gauze of nickel oxide layer and lies onto a NiO sheet, clearly visible on the left in the figure. The nickel elemental profile shows the presence of the sheet (from –100 nm to –50 nm) and

of the gauze (up to +100 nm). Beyond this limit (*i.e.* where the signal of nickel drops to zero), cobalt is probably oxidized because the gauze does not thoroughly cover the nanoparticle.

To conclude, it is possible to assert that starting with cobalt in the two-step process gives both Ni-core/Co-shell and Co-core/Ni-shell nanoparticles. The first kind of structure seems to be a bit less common (in number, maybe a half of the second kind) as far as the occurrence of both types of objects could be appreciated: the wrapping of one cobalt particle in a Nickel gauze is certainly more likely. Nickel seems to show an easier trend to form 2D structures as it also forms sheets whereas cobalt does not (only gauzes).

When the order is reversed and the process starts with nickel electrodes, both types of nanoparticles (Co and Ni) are detected as in the other experiments, but then Co_xNi_{1-x} alloy nanoparticles are also evidenced (TEM images in **Fig. 5**).

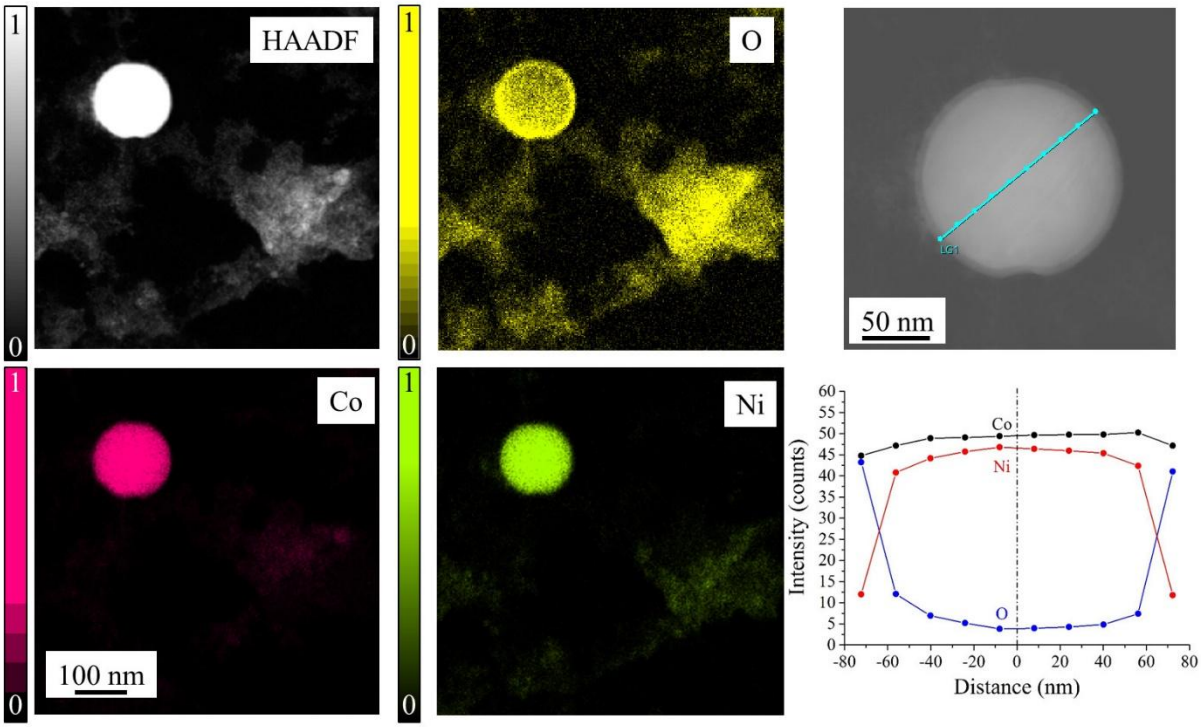

Fig. 5: STEM analysis of a CoNi alloy nanoparticle produced by a two-step process starting with one hour of pulsed discharges in Ni-Ni configuration followed by one hour of pulsed

discharges in Co-Co configuration. Coloured scales are normalized element intensities. Segregation of cobalt forming a CoO shell around the alloy nanoparticle is clearly visible.

Their composition is difficult to determine because of the presence of small nanoparticles forming a gauze that coats the studied particle. However, it is estimated to be close to $x = 50 \pm 10$ wt.%. The alloy is clearly oxidized and a layer depleted in nickel is observed around the core. For the same reason, the amount of nickel is difficult to determine. The elemental profile given in **Fig. 5** suggests the presence of nickel in the oxide shell but this measurement must be taken with caution. Indeed, the high-resolution image of the oxide shell shown in **Fig. 6** indicates that the shell is made of CoO. With a lattice parameter estimated to be 0.21 nm by averaging the distance over 10 atomic rows, the structure cannot compatible with the spinel structure of Co_3O_4.

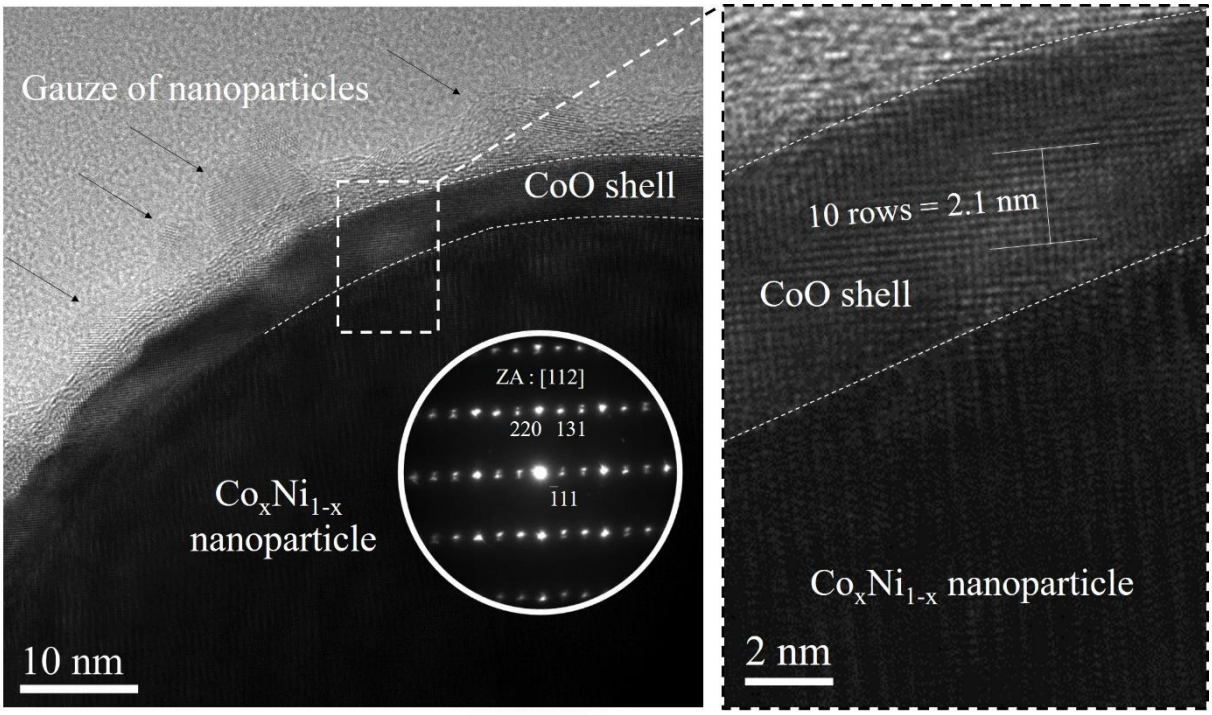

Fig. 6: HRTEM micrograph showing the edge of an alloy nanoparticle produced in a two-step process starting with nickel. The CoO shell is clearly visible and the gauze around contains nanoparticles (indicated by arrows). The lattice parameter of ~0.21 nm is not compatible with a spinel structure as Co_3O_4.

According to Law *et al.* [28], who studied oxidation of NiCo alloy by X-ray photoelectron spectroscopy, at very low pressure (5×10^{-7} mbar), CoO enriches the surface of the alloy with increasing annealing temperature. At high pressure (500 mbar), CoO is mainly found at low temperature whereas Co_3O_4 is formed at moderate temperature (around 500 K). With the formation of Co_3O_4, Ni^{2+} ions may exchange with Co^{2+} ions of the Co_3O_4 spinel, forming a layer of mixed nickel–cobalt spinel-like oxide. Thus, surface enrichment by cobalt is suppressed at high pressure and temperature. In our present conditions, the lack of nickel in the outermost part of the nanoparticle shell as seen in **Fig. 6** means that oxidation occurs at low temperature and in air (not during the process in liquid nitrogen), as explained previously. However, in this situation, oxygen should be present not only in the shell, but also in the core of the nanoparticle , which is clearly not what is found (**Fig. 5**). Let's also mention that no melting-point depression effect (*i.e.* the lowering of the melting temperature when the nanoparticle diameter decreases) must be expected with these large nanoparticles. We also confirm that no metallic nitrides have been observed.

3.3. Co-Ni mixed electrodes configuration

When a cobalt electrode faces a nickel electrode, besides NiO and CoO nanoparticles, alloy nanoparticles with sizes belonging to the three possible distributions are found (**Fig. 7** for medium and large particles – see **Supplemental Material 4** for an example of a small alloy nanoparticle –). For the first time, we show the possibility to produce alloy nanoparticles by gas phase condensation with nanosecond-pulsed discharges in liquid nitrogen, as a result of vapour mixing and condensation into alloys.

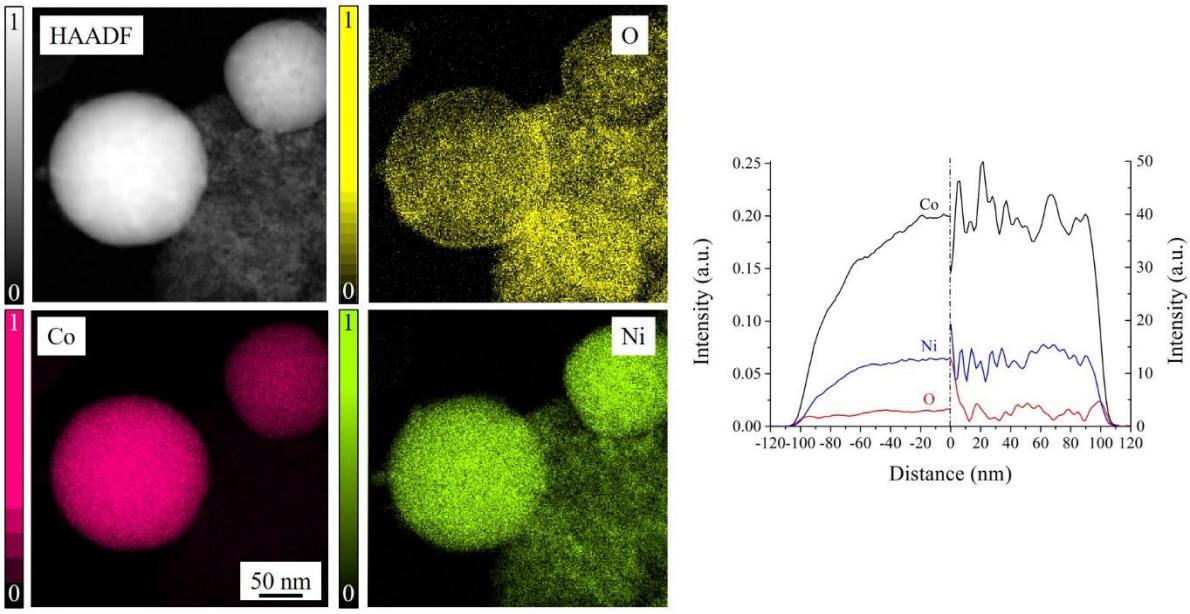

Fig. 7: STEM analysis of two CoNi alloy nanoparticles with large and medium size produced during one hour by pulsed discharges in Co-Ni configuration. Coloured scales are normalized element intensities. Smoothed and raw data intensities after Abel's inversion of elemental signals from HAADF measurements recorded along a line profile on the larger nanoparticle.

3.4. Growth mechanisms of alloy nanoparticles

As alloy nanoparticles belonging to each of the three possible size distributions are found, two situations must be distinguished:

- the synthesis of nanoparticles of small and medium sizes by gas phase condensation (only in the case of the one-step process with two different electrodes)
- the synthesis of large nanoparticles by emission of droplets from the liquid well (except in the case of the two-step process starting with cobalt electrodes).

Small and medium sizes

In the present conditions, 200 ns is typically the time scale needed to reach the melting point of most metals [29]. At shorter times (< 200 ns), vapours are likely emitted by another process, usually referred to as explosion of surface protrusions [30]. Usually, during the discharge process, vapours emitted by electrodes even with very different melting points are

expected to mix because of current oscillations that take place between electrodes at a frequency of several tens of MHz. The ion wind flowing back and forth within the inter-electrode gap allows for the mixing of vapours, as confirmed by time-resolved optical emission spectroscopy [15]. Therefore, vapour mixing would not be necessarily enhanced by the use of two metals with similar melting points. Furthermore, the mixing of vapours does not seem to lead straightforwardly to their alloying.

As demonstrated by Mattei *et al.* [31], the clustering rate of each elemental species is the primary limiting factor in the nanoparticle fabrication process used by these authors. The process is somewhat similar to the present one. Indeed, these authors used sputtering of two different targets, which is also a non-equilibrium discharge-based process with fast quenching rates. The same group showed by molecular dynamics simulations, in the silicon–silver binary system, that atoms of the emitted vapour first form independent clusters of Si and Ag without significant intermixing. Collisions between different species are unlikely in the early stages of growth (<100 ns), with large temperature differences resulting in rapid energy exchange and separation. Upon further cooling and depletion of isolated Si and Ag atoms through collection by parent clusters (>100 ns), Si−Ag cluster collisions ultimately result in stable hybrid structures [32]. So, as mentioned previously, a kind of incubation period is required that goes beyond the simple mixing of vapours of each element.

In the present experimental conditions, during the first 100 ns of the discharge, a vapour mixture is produced in which cobalt (or nickel) atoms start producing cobalt (or nickel) clusters. Subsequently, these parent clusters start aggregating to form alloy nanoparticles. This requires longer time periods during which both types of clusters co-exist. Since the duration of the plasma does not affect the respective proportions of each kind of nanoparticles (cobalt, nickel and alloy), the characteristic time of 100 ns meets quite well the residence time in the discharge before entering liquid nitrogen. This time scale is coherent with experiments performed with the shortest pulse width (75 ns) that is long enough to start observing alloy

nanoparticles. Unfortunately, shorter pulse widths could not be applied with the present experimental device.

Therefore, the synthesis of alloy is possible for particles with the longest residence time, those that are likely to be coming from the hottest part of the discharges (*i.e.* the farthest from liquid nitrogen). This, however, is a necessary but not sufficient condition for alloy formation. Indeed, the total miscibility between cobalt and nickel is also a crucial aspect of alloy nanoparticle formation because experiments made with copper and silver – two elements with quite close melting points too, respectively 1358 K and 1235 K – did not lead to the formation of alloys [33]. This also means that departure from equilibrium is probably very limited in the present process, thus the need for laser irradiation/melting to reach non-equilibrium conditions that are conducive to alloy formation [19].

On the other hand, condensation is likely submitted to specific conditions in order to synthesize alloy nanoparticles. Indeed, nanoparticles made either of nickel or cobalt are found in large amounts. The presence of alloy nanoparticles suggests that specific local conditions must exist to enable the mixing of elements into a single phase. At this stage, it sounds reasonable to admit that alloy nanoparticles must also be submitted to sufficiently fast quenching rates, *i.e.* in areas where temperatures are the highest, for no phase separation is observed in other non-fully miscible systems. Then, this feature of the synthesis process must be responsible for the presence of a high amount of defects in nanoparticles. Assuming a characteristic time of 100 ns and a plasma temperature of 1 eV [33], the thermal gradient is high: $\sim 1.1 \times 10^{11}$ K s^{-1}. However, by comparison, a quenching rate of the order of 10^{13} K s^{-1} is expected to get metastable silver-nickel alloy particles [34]. Yet, the actual gradient is pretty high anyway and must lead to the development of stress and the subsequent formation of defects in the particle structure. This is confirmed by results presented in **Fig. 8**. The presence of defects, and twins in particular, in Co_xNi_{1-x} alloy nanoparticles is depicted. Two lattices (in green and yellow) are observed in the diffraction pattern. They are twinned with respect to

each other. The green lattice (a variant of the twin defect) is indexed. Its zone axis is $[\bar{\mathbf{1}}\mathbf{01}]$. The yellow lattice is indexed with respect to the green one, which explains the presence of one third.

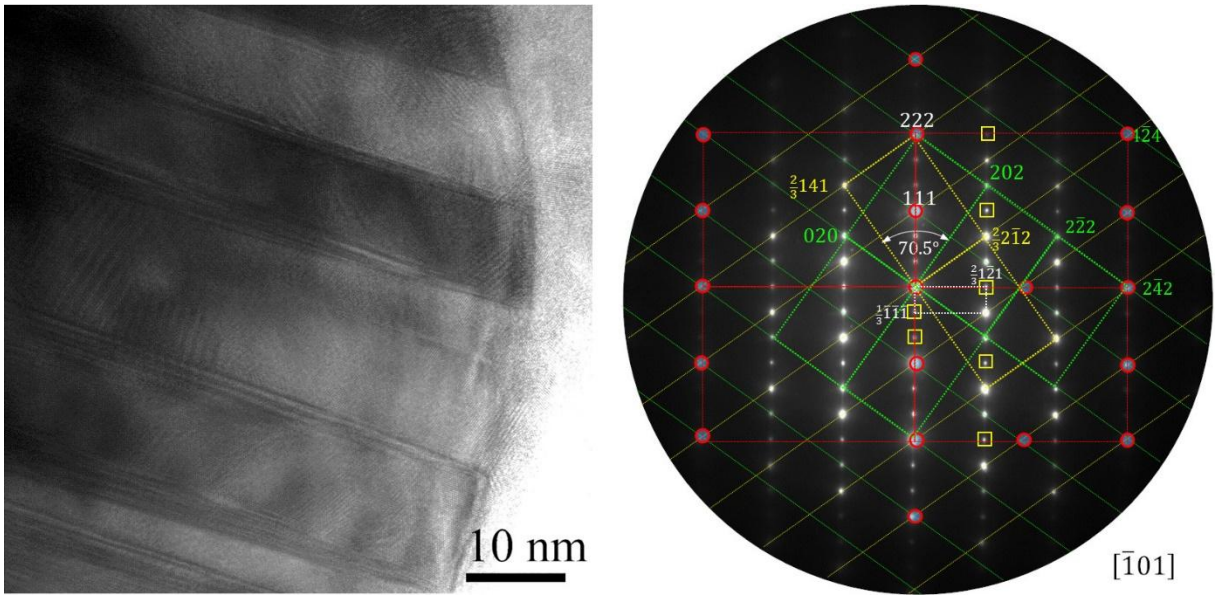

Fig. 8: TEM image of an alloy nanoparticles showing the presence of twin defects – laths in the left hand side figure. Electron diffraction pattern shows two lattices (in green and yellow) twinned one with respect to the other. Spots in red circles are those of the coincident site lattice.

The twinning plane, which belongs to both lattices is $(\mathbf{111})$. One can switch from one lattice to the other by a rotation of 70.5° around the $[\bar{\mathbf{1}}\mathbf{01}]$ axis (ZAP) or by a rotation of 180° around the $[\mathbf{111}]$ direction. Spots inside yellow squares are forbidden and are due to multiple diffractions. Spots in red circles are those of the coincident site lattice, Friedel's index is $\boldsymbol{\Sigma = 3}$. The twin boundary is thus $\boldsymbol{\Sigma 3}$. The lattice depicted with white dots represents the DSC (Displacement Shift Complete) lattice. Its base vectors are: $\frac{\mathbf{1}}{\mathbf{3}}\overline{\mathbf{111}}$ and $\frac{\mathbf{2}}{\mathbf{3}}\mathbf{1}\bar{\mathbf{2}}\mathbf{1}$ and given by linear combination the Burgers vectors of interfacial dislocations. Finally, we clearly observe the presence of patterns made of laths of 10 nm in width, which could be the former interfaces between nanoparticles before their clustering.

Large sizes

Let's consider now the possible mechanism responsible for the growth of the large alloy nanoparticles. Because they are large in size (typically around 100 nm), they are produced by ejection of liquid droplets from the well that forms at the electrode surface struck by the discharge and not by gas phase condensation, like the two other types of smaller particles studied before.

It is simple to understand how the liquid well of a given metal is enriched with the other metal in the one-step process. It is more complicated with the two-step process that leads to alloy nanoparticles only if nickel electrodes are used first. In this situation, as both electrodes are made of cobalt, the discharge is filled by a cobalt vapour and current oscillations are of no use to homogenize the vapour. So nickel, present as nanoparticles in the liquid outside the discharge region, must reach the electrode to access the liquid well and dissolve in the molten area from which droplets are emitted in order to produce the alloy. Nickel dissolves in liquid cobalt as efficiently as cobalt does in liquid nickel because the miscibility is total. So, the synthesis of alloy nanoparticles when the process starts by nickel is necessarily due to the presence made possible of nickel above the cobalt liquid well. The converse is not true: cobalt cannot be present above the nickel liquid well, otherwise alloy nanoparticles would be formed alike.

Two plausible reasons for this non-symmetrical behaviour between Co-Co/Ni-Ni and Ni-Ni/Co-Co two-step processes can be put forward.

- The first one is the sweeping effect by shockwaves that would not be efficient with nickel but with cobalt. So, the size distribution of particles must either enable or limit the presence in the inter-electrode gap. Nanoparticles are known to be repelled by shockwaves from the inter-electrode gap if their size makes it possible, *i.e.* if they are big enough. As described previously, the size distribution of the smallest particles is

lower for nickel (2 to 8 nm) than for cobalt (4 to 15 nm). By comparing these two ranges, the size threshold beyond which nanoparticles are blasted out of the discharge must be around 3 nm.

- The second one is the shape of the particles. Nickel particles are cubic whereas cobalt particles are spherical. As discussed in a previous paper [35], metallic particles with cubic shape present differential electrical charging, corners exhibiting opposite charges with respect to faces. For metallic spheres, charging is homogeneous. Nickel cubes are prone to be equally attracted by the fluctuating plasma potential – since it oscillates in the RF range as the current flow – contrary to the predominantly spherical cobalt nanoparticles [36].

Once the liquid well is enriched by another metal, ejection of droplets produces large (sub-micrometric) nanoparticles that are homogeneous in composition and quickly quenched in liquid nitrogen.

4. Conclusion

For the first time, we show the possibility for forming by nanosecond-pulsed discharges in liquid nitrogen alloy nanoparticles made of cobalt and nickel. Among single element nanoparticles that adopt specific shapes (nanocubes for nickel and nanospheres with facets for cobalt), one finds alloy nanoparticles belonging to the three possible size distributions.

Two mechanisms are needed to explain the synthesis of alloy nanoparticles. For nanoparticles with small and medium sizes, sufficiently-long residence times of species are needed to form primary clusters that mix after the incubation step. Then, they must be miscible to form alloys in conditions that are close to equilibrium. For sub-micrometric nanoparticles, the smallest nickel particles (around 3 nm and below) can enter the discharge region. They dissolve in cobalt wells to produce an alloy that can be ejected to form large alloy particles. Cobalt nanoparticles cannot enter the discharge created between nickel electrodes either because they

are too big and blasted out of the region by the shockwave or because they are not homogeneously charged, contrary to nickel nanocubes.

It is then quite clear that these processes are not fast enough to reach non-equilibrium conditions, which is possible by other processes like laser ablation in liquids. On the other hand, the production of sheets is frequently observed. Until now, no parameter (like surface energy, melting point, etc.) could have been identified to explain how these sheets are formed. It could be interesting to study more thoroughly this aspect to propose a realistic growth mechanism for these singular objects.

References

[1] G. Ennas, A. Falqui, G. Paschina and G. Marongiu, *Chem. Mater.* **2005**, *17*, 6486.

[2] H. L. Nguyen, L. E. M. Howard, G. W. Stinton, S. R. Giblin, B. K. Tanner, I. Terry, A. K. Hughes, I. M. Ross, A. Serres, J. S. O. Evans, *Chem. Mater.* **2006**, *18*, 6414.

[3] H. Zeng, J. Li, J. P. Liu, Z. L. Wang, S. Sun, *Nature* **2002**, *420*, 395.

[4] W. Chen, J. Kim, S. Sun, S. Chen, *Phys. Chem. Chem. Phys.* **2006**, *8*, 2779.

[5] F. Cheng, H. Ma, Y. Li, J. Chen, *Inorg. Chem.* **2007**, *46*, 788.

[6] R. Hong, N. O. Fischer, T. Emrick, V. M. Rotello, *Chem. Mater.* **2005**, *17*, 4617.

[7] W.-r. Lee, M. G. Kim, J.-r. Choi, J.-I. Park, S. J. Ko, S. J. Oh, J. Cheon, *J. Am. Chem. Soc.* **2005**, *127*, 16090.

[8] N. Panuthai, R. Savanglaa, P. Praserthdam, S. Kheawhom, *Jap. J. Appl. Phys.* **2014**, *53*, 05HA11.

[9] G. Saito, Y. Nakasugi, T. Yamashita, T. Akiyama, *Nanotechnol.* **2014**, *25*, 35603.

[10] S.-M. Kim, Y.-J. Lee, J.-W. Kim, S.-Y. Lee, *Thin Solid Films* **2014**, *572*, 260.

[11] P. Pootawang, N. Saito, O. Takai, S.-Y. Lee, *Nanotechnol.* **2012**, *23*, 395602.

[12] M. Mardanian, A.A. Nevar, M. Nedel'ko, N.V. Tarasenko, *Eur. Phys. J. D* **2013**, *67*, 208.

[13] H. Chang, M.-J. Kao, C.-S. Jwo, C.-G. Kuo, Y.-H. Yeh, W.-C. Tzeng, *J. Alloy. Comp.* **2010**, *504S*, S376.

[14] R. Rebiai, A.J. Rest, R.G. Scurlock, *Nature* **1983**, *305*, 412.

[15] H. Kabbara, J. Ghanbaja, C. Noël, T. Belmonte, *Mater. Chem. Phys.* **2018**, *207*, 350.

[16] H. Kabbara, J. Ghanbaja, C. Noël, T. Belmonte, *Mater. Chem. Phys.* **2018**, *217*, 371.

[17] H. Kabbara, C. Noël, J. Ghanbaja, K. Hussein, D. Mariotti, V. Švrček, T. Belmonte, *Sci. Rep.* **2015**, *5*, 17477.

[18] M. Trad, A. Nominé, N. Tarasenka, J. Ghanbaja, C. Noël, M. Tabbal, T. Belmonte,

Frontiers Chem. Sci. Eng. **2019**, *13*, 360.

[19] N.Tarasenka, A.Nevar, M. Nedelko, N. Tarasenko, A. Nominé, H. Kabbara, J. Ghanbaja, T. Belmonte, "Take the most of both: Synergistic effect of plasma and laser processes in liquid for alloyed nanoparticle synthesis", accepted in *Phys. Rev. Appl.*

[20] R. Xu, T. Xie, Y. Zhao, Y. Li, *Nanotechnol.* **2007**, *18*, 055602.

[21] F. Davar, Z. Fereshteh, M. Salavati-Niasari, *J. Alloys Comp.* **2009**, *476*, 797.

[22] M. Scariot, D. O. Silva, J. D. Scholten, G. Machado, S. R. Teixeira, M. A. Novak, G. Ebeling, J. Dupont, *Angewandte Chemie* **2008**, *47*, 9075.

[23] M. Shviro, D. Zitoun, *RSC Adv.* **2013**, *3*, 1380.

[24] Y.-P. Sun, H. W. Rollins, R. Guduru, *Chem. Mater.* **1999**, *11*, 7.

[25] A. Hamdan, C. Noel, F. Kosior, G. Henrion, T. Belmonte, *J. Appl. Phys.* **2013**, *113*, 043301.

[26] A. Hamdan, C. Noël, J. Ghanbaja, S. Migot-Choux, T. Belmonte, *Mater. Chem. Phys.* **2013**, *142*, 199.

[27] H. Kabbara, J. Ghanbaja, C. Noël, T. Belmonte, *Nano-Structures Nano-Objects* **2017**, *10*, 22.

[28] Y.T. Law, T. Dintzer, S. Zafeiratos, *Appl. Surf. Sci.* **2011**, *258*, 1480.

[29] A. Hamdan, F. Kosior, C. Noel, G. Henrion, J.-N. Audinot, T. Gries, T. Belmonte, *J. Appl. Phys.* **2013**, *113*, 213303.

[30] P. Bruggeman, C. Leys, *J. Phys. D: Appl. Phys.* **2009**, *42*, 053001.

[31] J.-G. Mattei, P. Grammatikopoulos, J. Zhao, V. Singh, J. Vernieres, S. Steinhauer, A. Porkovich, E. Danielson; K. Nordlund, F. Djurabekova, M. Sowwan, *Chem. Mater.* **2019**, *31*, 2151.

[32] V. Singh, C. Cassidy, P. Grammatikopoulos, F. Djurabekova, K. Nordlund, M. Sowwan, *J. Phys. Chem. C* **2014**, *118*, 13869.

[33] T. Belmonte, H. Kabbara, C. Noël, R. Pflieger, *Plasma Sources Sci. Technol.* **2018**, *27*, 074004.

[34] D. Poondi, J. Singh, *J. Mater. Sci.* **2000**, *35*, 2467.

[35] M. Trad, A. Nominé, N. Tarasenka, J. Ghanbaja, C. Noël, M. Tabbal, T. Belmonte, *Front. Chem. Sci. Engin.* **2019**, *13*, 360.

[36] K. McCreery, H. Greenside, arXiv **2016**, 1607.07703.

CAPTIONS

Fig. 1: Nickel and cobalt nanoparticles observed by transmission electron microscopy at different magnifications. Nickel oxide nanoparticles are cubic with sizes below 10 nm. Cobalt oxide nanoparticles appear more spherical and exhibit three size distributions, as discussed in the text.

Fig. 2: TEM micrographs of cobalt and nickel nanoparticles observed after a two-step process starting with one hour of pulsed discharges in Co-Co configuration followed by one hour of pulsed discharges in Ni-Ni configuration.

Fig. 3: STEM analysis of a nickel nanoparticle covered by cobalt oxide obtained by a two-step process starting with Co. Coloured scales are normalized element intensities. Elemental analysis (on the rhs of the figure) along a line depicted in the HAADF image shows clearly constant intensities of O and Co, contrary to nickel (top graph). The actual distribution of elements within the particle can be deduced by Abel's inversion (bottom graph – see main text for details). It is clearly a Ni-core/CoO-shell structure. The nickel nanoparticle is wrapped into a CoO gauze. It is not a segregation of cobalt in a CoNi alloy leading to a CoO layer with a core depleted in cobalt as it will be described hereafter. The distribution of cobalt over the nickel nanoparticle is not necessarily homogeneous.

Fig. 4: STEM analysis of a cobalt nanoparticle produced by a two-step process starting with Co. Coloured scales are normalized element intensities. The nanoparticle is covered by a gauze of nickel oxide layer and lies onto a NiO sheet, clearly visible on the left in the figure. The nickel elemental profile shows the presence of the sheet (from −100 nm to −50 µm) and of the gauze (up to +100 µm). Beyond this limit (*i.e.* where the signal of nickel drops to zero), cobalt is probably oxidized because the gauze does not thoroughly cover the nanoparticle.

Fig. 5: STEM analysis of a CoNi alloy nanoparticle produced by a two-step process starting with one hour of pulsed discharges in Ni-Ni configuration followed by one hour of pulsed

discharges in Co-Co configuration. Coloured scales are normalized element intensities. Segregation of cobalt forming a CoO shell around the alloy nanoparticle is clearly visible.

Fig. 6: HRTEM micrograph showing the edge of an alloy nanoparticle produced in a two-step process starting with nickel. The CoO shell is clearly visible and the gauze around contains nanoparticles (indicated by arrows). The lattice parameter of ~0.21 nm is not compatible with a spinel structure as Co_3O_4.

Fig. 7: STEM analysis of two CoNi alloy nanoparticles with large and medium size produced during one hour by pulsed discharges in Co-Ni configuration. Coloured scales are normalized element intensities. Smoothed and raw data intensities after Abel's inversion of elemental signals from HAADF measurements recorded along a line profile on the larger nanoparticle. Smoothed and raw data after Abel's inversion of elemental signals from a line profile on the larger nanoparticle.

Fig. 8: TEM image of an alloy nanoparticles showing the presence of twin defects – laths in the left hand side figure. Electron diffraction pattern shows two lattices (in green and yellow) twinned one with respect to the other. Spots in red circles are those of the coincident site lattice.

Table of Contents

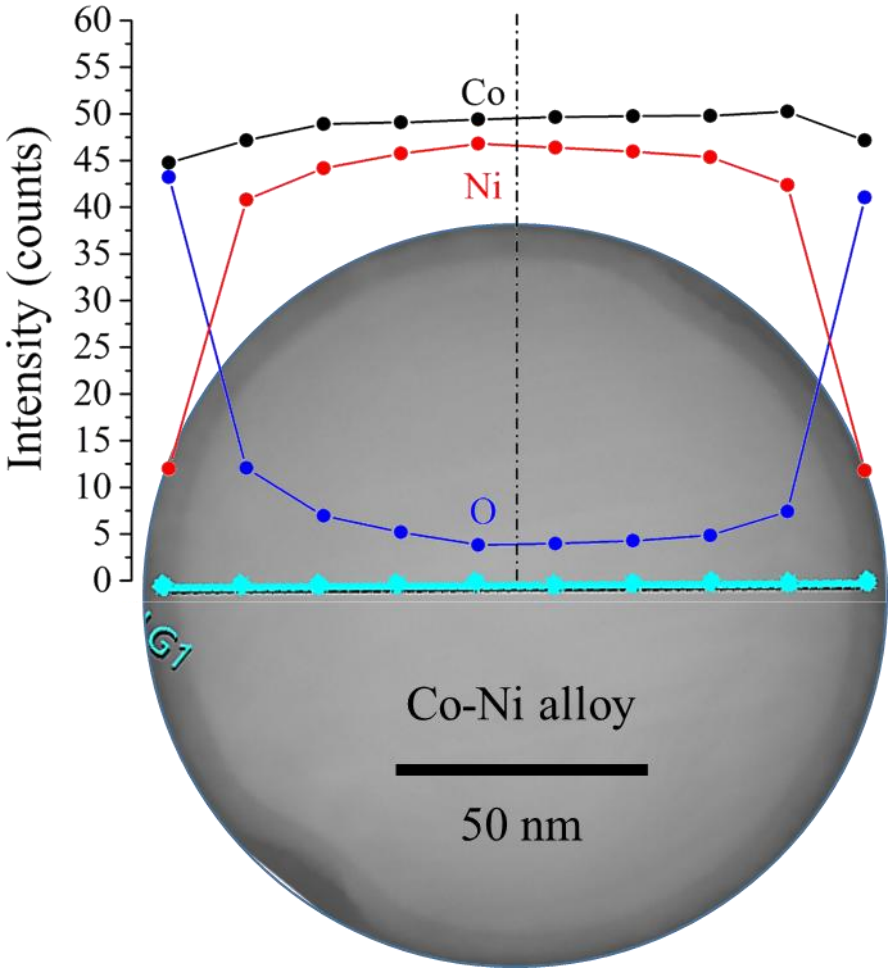

CoNi alloy nanoparticle produced by a two-step process starting with one hour of pulsed discharges in Ni-Ni configuration followed by one hour of pulsed discharges in Co-Co configuration. Elemental analysis is plotted along a diameter. Segregation of cobalt forming a CoO shell around the alloy nanoparticle is clearly visible.

SUPPLEMENTAL MATERIAL 1

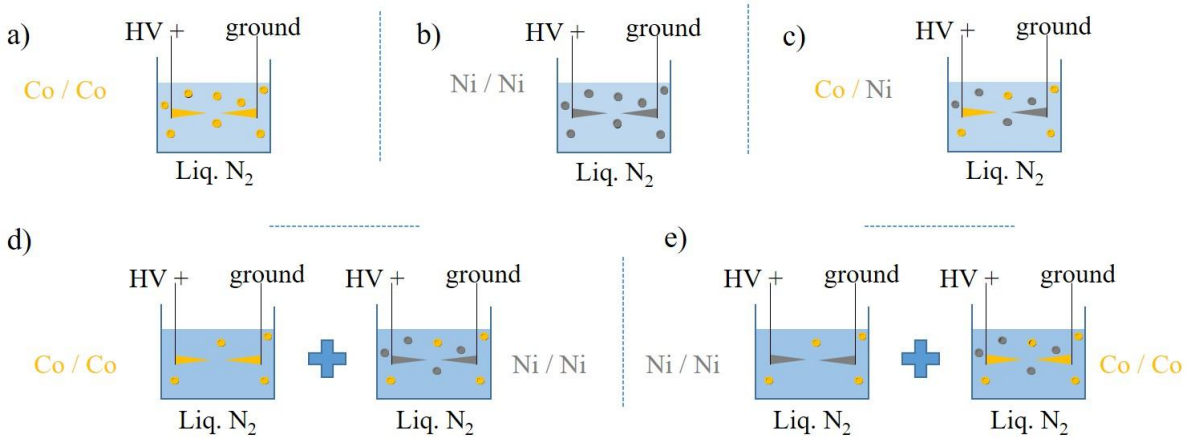

Fig. S1: Different arrangements of electrodes used. 18000 discharges are run for each step whatever the configuration. The total treatment time is 30 min for a one-step process and 60 min for a two-step process.

SUPPLEMENTAL MATERIAL 2

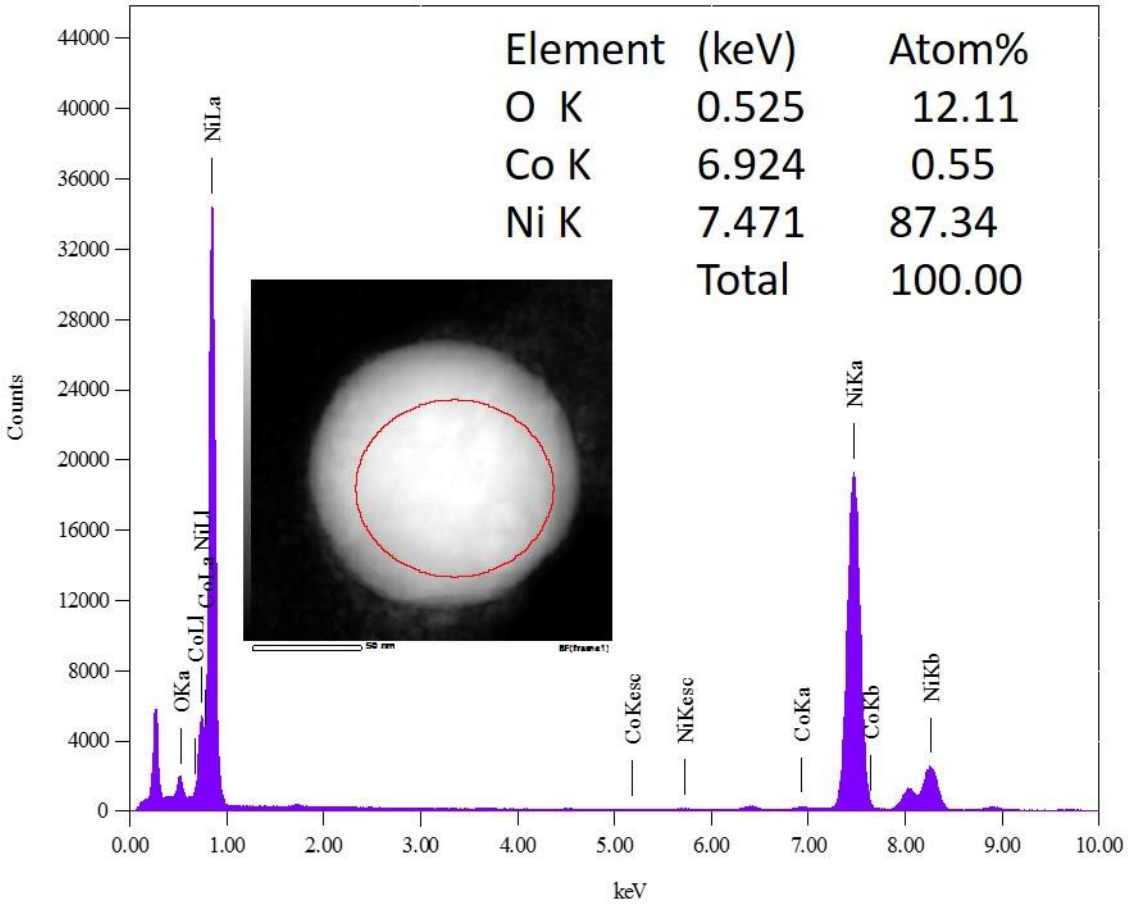

Fig. S2: Micro-EDX analysis of a nickel nanoparticle (the same as in **Fig. 3**) covered by cobalt oxide obtained by a two-step process starting with Co.

SUPPLEMENTAL MATERIAL 3

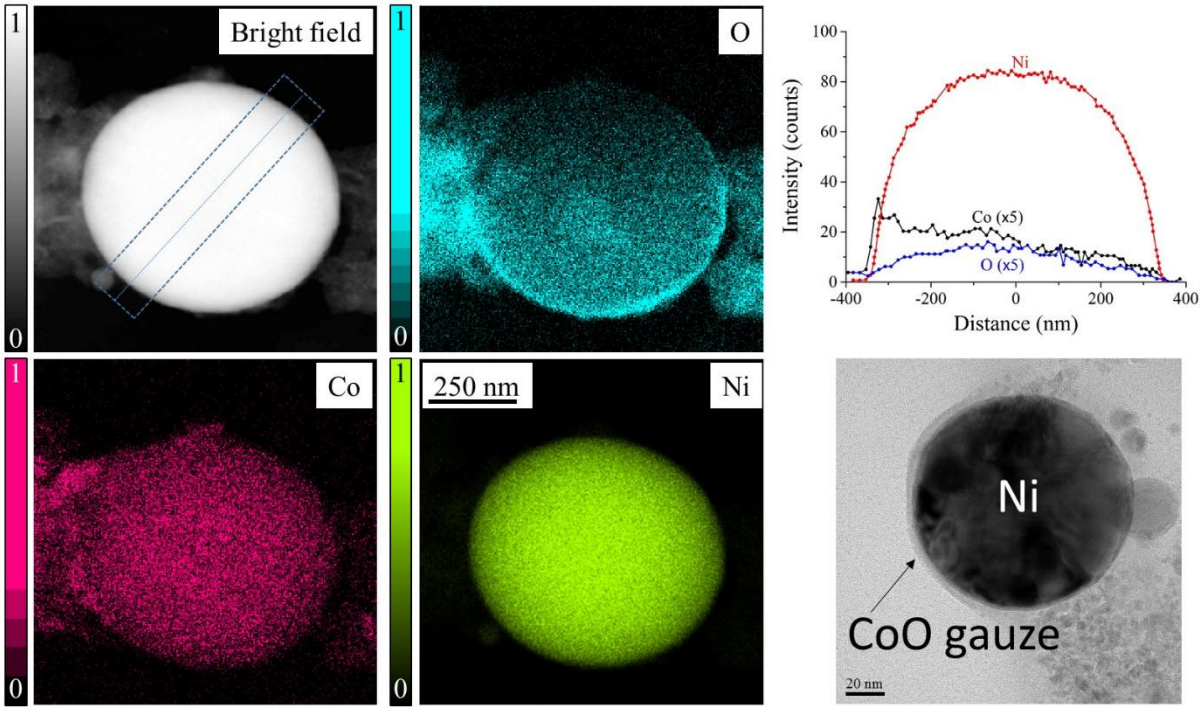

Fig. S3: Example of a nickel nanoparticle partially wrapped in a CoO gauze. The elemental profiles show the asymmetry of cobalt distribution due to the presence of the gauze only on one side of the particle.

SUPPLEMENTAL MATERIAL 4

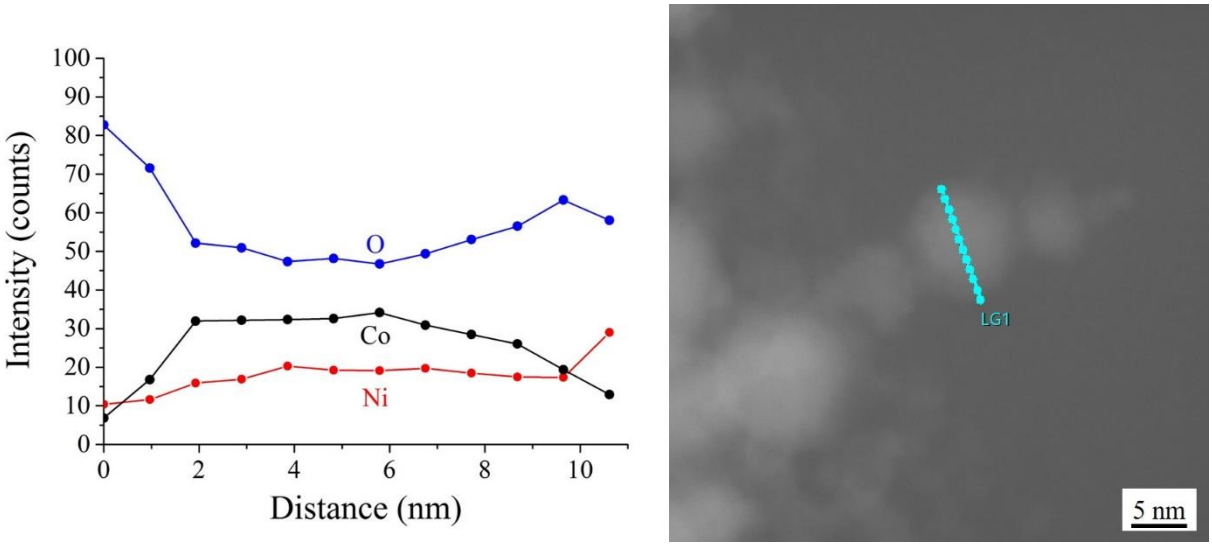

Fig. S4: Elemental profiles of a small Co_xNi_{1-x} alloy nanoparticle produced by discharges between one nickel electrode and one cobalt electrode.